Self-Assembled Large Au Nanoparticle Arrays with Regular Hot Spots for SERS

Aiqing Chen, A. Eugene DePrince III, Arnaud Demortière, Alexandra Joshi-Imre, Elena V. Shevchenko, Stephen K. Gray, Ulrich Welp, and Vitalii K. Vlasko-Vlasov**

The cost-effective self-assembly of 80 nm Au nanoparticles (NPs) into large-domain, hexagonally close-packed arrays for high-sensitivity and high-fidelity surface-enhanced Raman spectroscopy (SERS) is demonstrated. These arrays exhibit specific optical resonances due to strong interparticle coupling, which are well reproduced by finite-difference time-domain (FDTD) simulations. The gaps between NPs form a regular lattice of hot spots that enable a large amplification of both photoluminescence and Raman signals. At smaller wavelengths the hot spots are extended away from the minimum-gap positions, which allows SERS of larger analytes that do not fit into small gaps. Using CdSe quantum dots (QDs) a 3–5 times larger photoluminescence enhancement than previously reported is experimentally demonstrated and an unambiguous estimate of the electromagnetic SERS enhancement factor of $\approx 10^4$ is obtained by direct scanning electron microscopy imaging of QDs responsible for the Raman signal. Much stronger enhancement of $\approx 10^8$ is obtained at larger wavelengths for benzenethiol molecules penetrating the NP gaps.

1. Introduction

Surface-enhanced Raman spectroscopy (SERS) is a fast-developing optical technique for the detection and identification of nanoscale quantities of chemical and biological analytes using their distinctive vibrational modes. Its unique sensitivity capable of single-molecule detection is largely based on the strong enhancement of the light intensity in hot spots—subnanometer features on nanostructured metal surfaces and aggregates of metal nanoparticles (NPs).[1,2] The main challenge in the development of SERS-based detectors is the creation of SERS-active substrates with well-controlled arrays of hot spots yielding light-field enhancement in an efficient and reproducible way. Traditional SERS substrates, such as rough metal films and NP colloids, carry randomly distributed hot spots, which results in low fidelity of the Raman signals. A possible solution could be the use of electron-beam lithography (EBL), which allows for the production of regular nanopatterns for SERS.[3] However, the consistent EBL fabrication of high-density subnanometer gaps over reasonably large areas is not yet practical. An alternative is nanosphere lithography, in which self-assembled dielectric NPs serve as templates for depositing a conforming lattice of metallic nanoislands.[4] Regular assemblies of colloidal metal NPs are also considered as a promising platform for SERS devices.[5,6]

Different nanostructures including three-dimensional designs offer considerable improvement of the enhancement factors.[7] Our focus here, however, will be on two-dimensional substrates that we believe have advantages in terms of overall sensitivity and fidelity, and easy analyte deposition. For plasmonic applications requiring strong amplification of light, the choice is usually gold or silver NPs with large diameters (>30–50 nm), which have low optical losses and allow a large number of electrons to participate in the local plasmon resonances, thereby yielding a strong enhancement of the

Dr. A. Chen, Dr. U. Welp, Dr. V. K. Vlasko-Vlasov
Materials Science Division
Argonne National Laboratory
Argonne, IL 60439, USA
E-mail: aiqingchen@anl.gov; vlasko-vlasov@anl.gov
Dr. A. E. DePrince III, Dr. A. Demortière, Dr. A. Joshi-Imre,
Dr. E. V. Shevchenko, Dr. S. K. Gray
Center for Nanoscale Materials
Argonne National Laboratory
Argonne, IL 60439, USA

DOI: 10.1002/smll.201100686

light intensity. Larger NPs can have advantages for SERS; for example, such NPs have larger absorption and scattering cross sections,[8] which could be favorable for SERS.[7,9] However, manufacturing extended arrays of large metal NPs, commonly implemented through capillary self-assembly, turns out to be much more difficult than the assembly of dielectric NPs and small (<10 nm) metal NPs. First, it is not easy to synthesize and stabilize large Au and Ag NPs with a well-defined shape and monodispersity. Second, the assembly of large metal NPs is more sensitive to gravity, which causes a faster sedimentation rate and stronger friction against the substrate. Also, it is hard to keep the uniformity of large metal NP colloids during the lengthy self-assembly process. All these factors hinder the formation of large ordered domains. Therefore, conventional methods such as dip-coating assembly, which employs a slow retraction of the substrate from a NP solution, or solvent evaporation[10] are ineffective in the case of large metal NPs.

Herein, we demonstrate the simple and cost-effective large-scale self-assembly of large (80 nm) colloidal Au NP arrays with regular ≈1 nm gaps and extended up to a few hundred micrometers, which is noticeably larger than monocrystalline areas previously reported for such large particles.[11] We show that optical spectra of the arrays are modified by the strong coupling between Au NPs, as confirmed by our finite-difference time-domain (FDTD) calculations. We find a strong light amplification in our structures by measuring SERS and photoluminescence (PL) signals of 5 nm CdSe quantum dots (QDs) and directly evaluate the enhancement factors by imaging and counting QD reporters using high-resolution scanning electron microscopy (SEM). This procedure yields a moderate electromagnetic SERS enhancement of 10^4 for relatively large QDs occupying regions outside the narrowest gap. In spite of that, our design, which benefits from the extension of the high-intensity regions between large NPs and the large density of the periodic hot spots, provides strong and stable Raman signals from few-micrometer areas. The advantages of the high uniform density of hot spots, their easy access for analytes, and a cost-effective self-assembly process for their manufacture show the potential of large NP arrays for SERS applications. Their ability to generate a much larger enhancement factor of $\approx 10^8$ is confirmed at higher excitation wavelengths for benzenethiol (BT) molecules filling the interparticle gaps.

2. Results and Discussion

In this work, large ordered Au NP arrays on planar silicon substrates and indium tin oxide (ITO)-covered glass slides were fabricated by solvent evaporation in a Teflon ferrule. This approach was successfully used for the assembly of large colloidal crystals of polystyrene particles with 47 nm to 2 μm diameters.[12] To implement this technique for the assembly of large Au NPs, we experimentally adjusted key parameters controlling the process, such as NP concentration, surface tension and purity of the solvent, the evaporation rate, and number of capping ligands on the NP surface. We used 80 nm Au NPs from Ted Pella and tuned the thickness of their capping ligand layer (the composition of ligands is proprietary information of Ted Pella) by several cycles of centrifugation followed by the replacement of the solvent with deionized water (18.2 MΩ cm). The purified and concentrated colloidal solution of Au NPs was then injected into a Teflon ferrule glued with rubber cement on Si or ITO-covered glass substrates, as shown in **Figure 1**a. The ferrule was covered with a glass slip to reduce the evaporation rate and the self-assembly process was monitored using an optical microscope and computer-controlled digital camera. In the course of drying, the colloidal droplet acquired a concave shape with a minimum thickness in the center of the ferrule. When the depth of the thinning water layer became equal to the particle diameter, capillary interactions forced the Au NPs to start assembling at the liquid/substrate contact line. This process is similar to the colloidal assembly of polystyrene spheres.[13] Convective flow induced by solvent evaporation at the drying front dragged NPs from the bulk of the

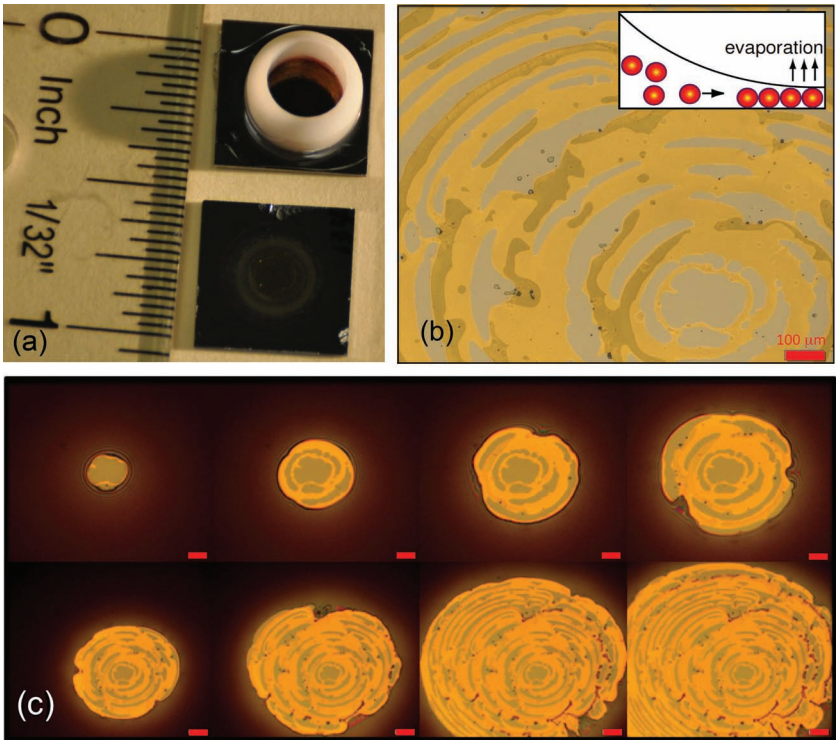

Figure 1. a) Teflon ferrule glued on the ½-inch Si substrate with rubber cement. b) Optical image of the 80 nm Au NP arrays (monolayers of NPs: light beige, double layers: dark beige, and bare Si: gray). The inset shows a scheme of the NP assembly during solvent evaporation. c) Sequence of frames illustrating the self-assembly of 80 nm Au NPs from the water solution. The meniscus of the liquid colloid (purple) moves from the center of the ferrule to the periphery. Intervals between the frames are 500 s in the top row and 5000 s in the bottom row. Scale bar: 200 μm.

NANO MICRO small

solution towards the contact line, thereby assisting the crystal growth there (see inset in Figure 1b). Depending on the particle concentration, a monolayer or multiple layers were deposited. Usually, the number of layers increased abruptly from one to two during the crystal assembly. As shown in Figure 1b, monolayer and double-layer bands formed quasi-periodically along the direction of the meniscus motion, alternating with empty bands. Such a banding process is often observed in capillary self-assembly experiments and is associated with the stick–slip motion of the contact line.[14–16] Figure 1c presents a typical sequence of pictures appearing during the drying process. Images were taken in 10 s intervals using an Olympus X61 microscope with a long-distance 5× objective. The NP concentration had a strong effect on the band spacing and could essentially change the geometry of the pattern (Supporting Information (SI), Figure S1).

Our experiments showed that the assembly process is very sensitive to this cleaning procedure. After an excess removal of the ligands, the NPs aggregate as shown in **Figure 2**a. However, insufficient cleaning leads to a strong repulsion of the NPs and their dispersion on the substrate, as illustrated in Figure 2b. After a few cycles of centrifugation (see Experimental Section) and final dilution to a concentration of ≈1.0×10^{11} mL^{-1} and 30–50 μL initial solution volume, we obtained few-millimeter-long and, on average, more than 100-μm-wide bands. The SEM image in Figure 2c shows a high degree of ordering in the bands, which is surprising given the large NP diameter scatter in the colloid used (7% monodispersity). Based on the recorded movie, we find a stable self-assembly speed of ≈0.1 μm s^{-1} for a monolayer and 0.03 μm s^{-1} for a double layer. The glass cover on the ferrule, which controlled the slow evaporation rate, assisted the formation of uniform crystalline structures and allowed us to obtain extended Au NP crystals over 200×1000 μm^2 areas, as shown in Figure 2c. The close-up in Figure 2d and fast Fourier transform (FFT) image in the inset confirm the good ordering of the structure.

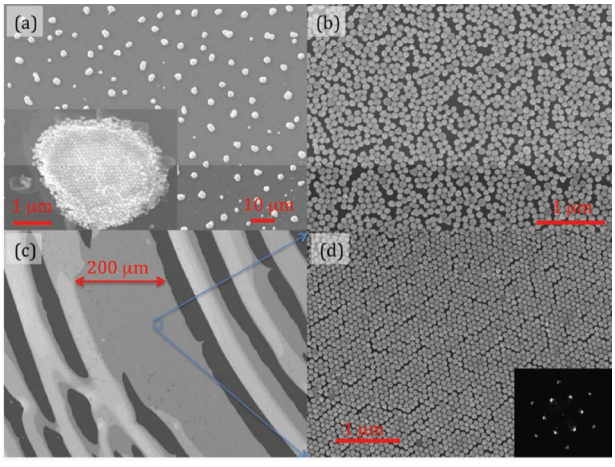

Figure 2. SEM images of 80 nm Au NPs assembled under different conditions. a) Aggregation of NPs after the excess clean-up of ligands (the inset shows a close-up view). b) Disordered monolayer of NPs formed after insufficient clean-up of ligands. c,d) Hexagonal close-packed (hcp) NP arrays obtained after tuning the clean-up procedure. The FFT pattern in the inset confirms good ordering of the NPs.

The whole area appears to be a single domain, although it contains linear "cracks" of slightly increased gaps between the particles. This is a typical feature of the evaporative assembly technique.

Figure 3a shows the extinction spectra of an 80 nm Au NP colloid in a cuvette and of disordered and ordered Au NPs deposited on transparent ITO-covered glass substrates. The extinction is defined as the negative logarithm of light intensity transmitted through the NP arrays normalized by the intensity transmitted through the pure substrate. While the aqueous Au NP colloid exhibits a single resonance near 550 nm, consistent with a dipolar Mie scattering on individual Au NPs, ordered Au NP monolayers show a double resonance structure associated with a strong coupling between NPs. Large individual Au NPs can also show spectra with double maxima, where one of the resonances represents the red-shifted dipolar mode and the other corresponds to a

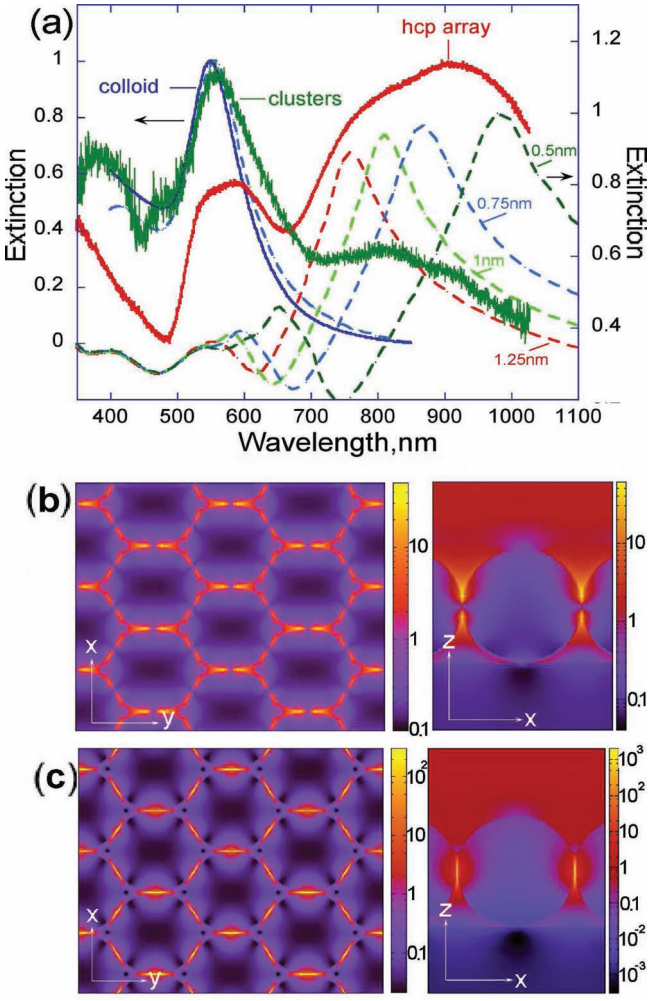

Figure 3. a) Extinction spectra (normalized by maximum value) of the aqueous colloid of 80 nm Au NPs (blue), Au NP hcp arrays on ITO-coated glass (red), and Au NP aggregates on ITO-coated glass (green). The dashed lines show FDTD calculated spectra of the colloid and ordered NP array with 0.5–1.25 nm gaps. b,c) Simulated light enhancement (E^2/E_0^2 –incident) in the *x*–*y* and *x*–*z* planes crossing the centers of NPs, at 514 nm ("blue" resonance region) and 835 nm ("red" resonance) at 1 nm gap. *z* is the incidence direction of *x*-polarized light.

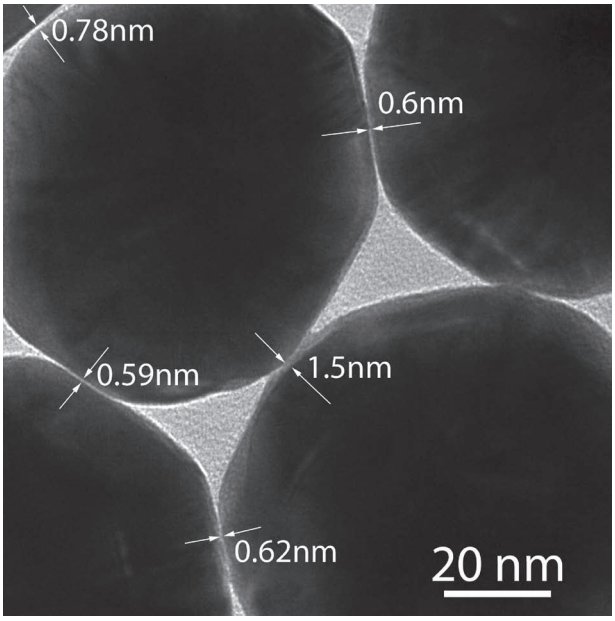

Figure 4. High-resolution TEM image showing the distribution of interparticle gaps between 80 nm Au arrays.

developing blue-shifted quadrupolar mode.[17] However, in the NP arrays the situation is more intricate. Here the resonances are formed by a series of interacting multipolar modes of the particles and coupling to the substrate. The results of FDTD calculations in Figure 3a–c, which incorporate the geometrical details of our NP arrays and the 20 nm ITO/glass substrate, are in good agreement with the experimental spectra and show complex light-field patterns in the NP array at the "blue" (around ≈550 nm) and the "red" (around ≈850 nm) resonances. The double hump structure of the measured "red" spectral maximum in Figure 3a can be well reproduced by assuming variations of the interparticle gap between ≈0.6 and ≈1 nm (see broken lines in Figure 3a), in agreement with our transmission electron microscopy (TEM) estimates of the interparticle gaps (**Figure 4**). At the same time, the "blue" resonance is intrinsically constructed of two overlapping modes with different field patterns. Their splitting increases with decreasing interparticle gap. For a 1 nm gap these modes are at ≈520 and ≈585 nm. In contrast, the disordered Au aggregates show a broadened single-particle dipolar mode and strongly suppressed peak around ≈850 nm, which indicates a lack of long-range coupling.

It was reported recently that electromagnetic hot spots in the subnanometer gaps of large (≈50 nm) Au NP trimers can provide a SERS enhancement factor of $\approx 10^8$ in a wide range of frequencies near their plasmon resonances.[18] This enhancement was strongly dependent on the gap size and was dominated by individual interparticle junctions. Multiple regular hot spots in our hcp structures offer a high average SERS sensitivity. We estimated the enhancement factor in different parts of our samples, where monolayer and double-layer NP assemblies and also bare substrate were distinguished by their contrast in reflected light. CdSe QDs (5 nm), which ensure good optical stability and low blinking and bleaching effect, were used as SERS reporters. An important advantage of these QDs is the possibility of resolving them with SEM so that their density and positions in our Au NP arrays can be directly imaged. Also, they show a good PL yield, which allows us to measure the PL enhancement factor in the NP arrays. CdSe QDs were synthesized using the trioctylphosphine/trioctylphosphine oxide (TOP/TOPO) capping method[19,20] with good NP size control (SI, C). **Figure 5**a shows spectra of a dilute (0.5×10^{-4} mol L^{-1}) solution of CdSe QDs in toluene with well-resolved absorption and emission lines at 600 and 620 nm, respectively, indicative of a narrow size distribution (6%).[21] TEM images (SI Figure S2) show that QDs have a shape of slightly prolate spheroids with an average diameter of 5 nm. The PL quantum yield of these particles has been estimated at 5%.[22]

To determine the PL enhancement, a 100 nM solution of CdSe QDs in toluene was drop-coated over the Au NP arrays, as shown in Figure 5b. (Much lower QD concentrations yield no PL or Raman signal from the silicon surface, our reference for inferring enhancement factors, although we do obtain signals from our Au arrays.) The drying drop forms a "coffee-ring" pattern with increased density of particles and organic ligands at the periphery (stained region in Figure 5b) on the Au monolayer (light beige), double layer (dark beige), and pure Si (blue). Figure 5c shows the PL image of the CdSe QDs under UV illumination. Scans of the PL signal show up to 10 times higher intensity on the Au NP arrays (in both single- and double-layer areas) than in the bare Si stripes with the same QD density (SI, Figure S3). This value is ≈3–5 times higher than that previously reported for CdSe/ZnS core/shell QDs[23] and CdSe QDs on disordered ≈15 nm Au NP assemblies with optimized dielectric spacer thickness.[24]

Figure 5d shows the Raman spectra of CdSe QDs collected in different spots of the red box in Figure 5b. The red curve is the SERS signal of the CdSe QDs on the Au monolayer and the blue curve is the signal on bare silicon substrate. Both spectra were collected under the same acquisition conditions in the spots shown by arrows in Figure 5d. After extraction of the background, the Raman peak at 207 cm^{-1} of the CdSe QDs deposited on the Au array is 500 times higher than that on silicon. This characteristic peak corresponds to the CdSe longitudinal optical phonon mode—LO(1).[25] Also, the second harmonic of this vibrational mode, –2LO(1), near 414 cm^{-1} is clearly seen on Au NPs but is not resolved for QDs on silicon. The QD Raman peaks in Figure 5d are more pronounced than those measured in commercial plasmonic arrays of inverted pyramids (Klarite substrates) excited at the same 514 nm wavelength.[26] The 2D Raman scan image at 207 cm^{-1} (inset in Figure 5d) clearly visualizes the enhancement of the SERS signal on the Au NP arrays. The high-resolution SEM images in Figure 5e,f reveal the same areal density of QDs on bare Si and on the Au arrays.

We used SEM images of the QDs on the NPs and electric field maps, such as shown in Figure 3b, to determine the number of QDs situated in the highest local fields, since these QDs are likely to dominate the SERS signal. At 514 nm excitation the maximum electric fields are located approximately 10 nm away from the positions of the smallest gap between NPs. Such a symmetry of the 514 nm resonance, different from dipolar or quadrupolar modes of separated NPs, is

small NANO MICRO

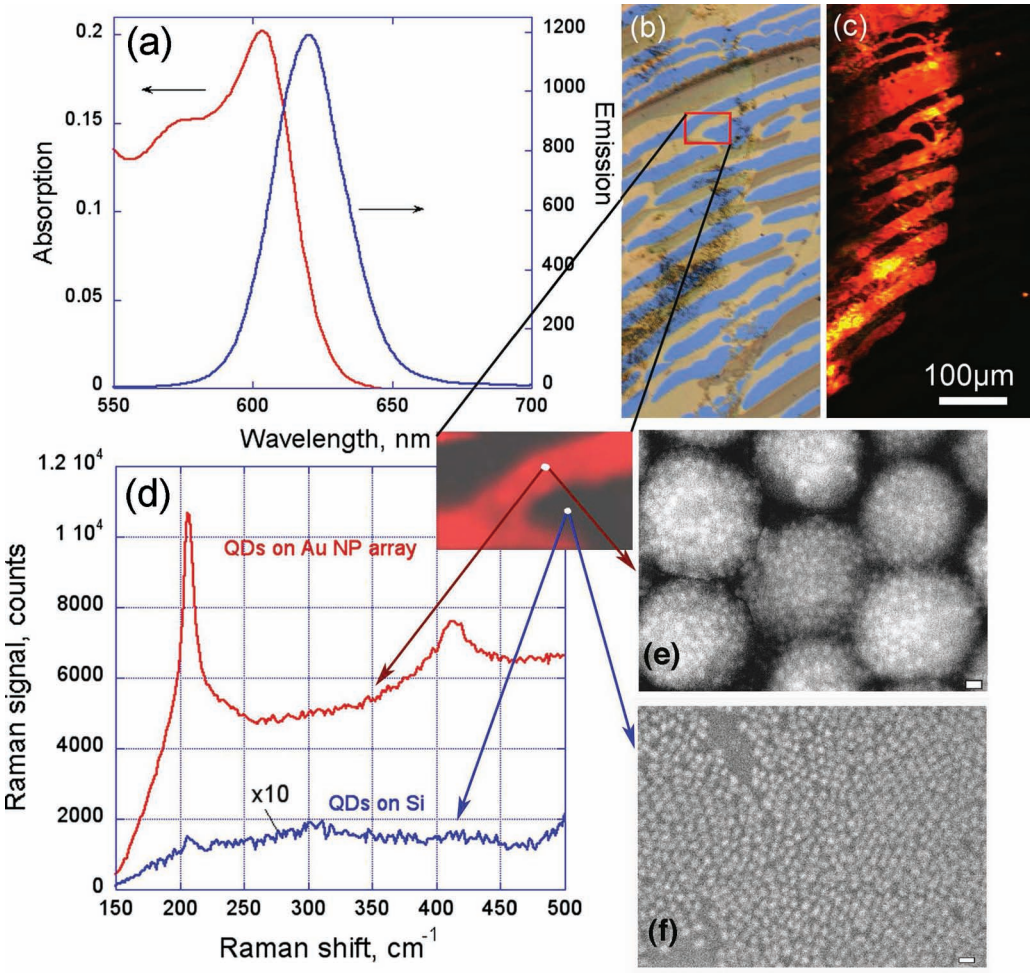

Figure 5. a) Absorption and emission spectra of 5 nm CdSe QDs. b) Optical image of the sample surface with a dried ring of QDs covering bands of the Au NP monolayers (light beige), double layers (dark beige), and bare Si (blue). Dark deposits are dried ligands from the solvent. c) PL image of the area shown in (b). d) SERS spectra of the QDs on the Au NP monolayer (red curve) and on bare Si (blue curve, the signal is multiplied by 10). The inset shows a 2D SERS scan at the 207 cm^{-1} peak wavelength. The scan area is outlined by the red box in (b). Arrows point to the SERS spectra acquisition spots. e,f) SEM images in these spots reveal the same density of QDs on Au NPs (e) and on bare Si (f). Scale bars in (e) and (f): 10 nm.

very beneficial for our SERS experiment since 5 nm particles would not fit into the gap. The evaluation of this geometry yields that about 5% of the QDs are located in places of maximum electric field corresponding to a SERS gain of $\approx 10^4$. Note the enhancement factor in question is associated with the volume of a hot spot, that is, it is not an average over all QDs, many of which are not in hot spots and not undergoing appreciable Raman scattering.[27] This enhancement factor is a few orders of magnitude lower than those reported by others for clusters of colloidal metal NPs.[11,18] However, in our case the number and positions of the QDs are directly visualized using high-resolution SEM, which eliminates the common problem of uncertainty in the analyte molecule density and location inherent for most experimental estimates of the SERS enhancement. Therefore, we obtain a reliable value of the enhancement factor, which is in a good agreement with the results of our FDTD simulations. For 514 nm they predict maximum amplification of the light intensity, $|E|^2$, $\approx 10^2$ at ≈10 nm above the center of 1 nm gaps between NPs (see Figure 3b), which corresponds to a SERS enhancement of $\approx 10^4$. For 830 nm excitation wavelength, located in the region of the strong resonance peak (Figure 3a), we calculate $\approx 10^3$ times larger SERS enhancement. However, even at 514 nm the high density of regular hot spots in our arrays significantly increases their practical sensitivity, thus allowing the detection of tiny amounts of chemical analytes.

To realize larger SERS enhancement we covered our NP arrays with BT by soaking them for 12 h in 1 mM BT solution in ethanol and subsequently rinsing with pure ethanol. Such a procedure is known to form a continuous monolayer of BT molecules with $4.3–6.8 \times 10^{14}$ molecules per cm^2 surface coverage.[28–30] The monolayer thickness of 0.6–0.8 nm estimated by X-ray photoelectron spectroscopy suggests good filling of the interparticle gaps. Also, for BT we used the largest excitation wavelength, 633 nm, available in our system, which provided higher light intensities in the gaps compared to 514 nm and a strong Raman signal, as shown in **Figure 6**. We did not see any Raman peaks from BT on flat glass or Au films. The

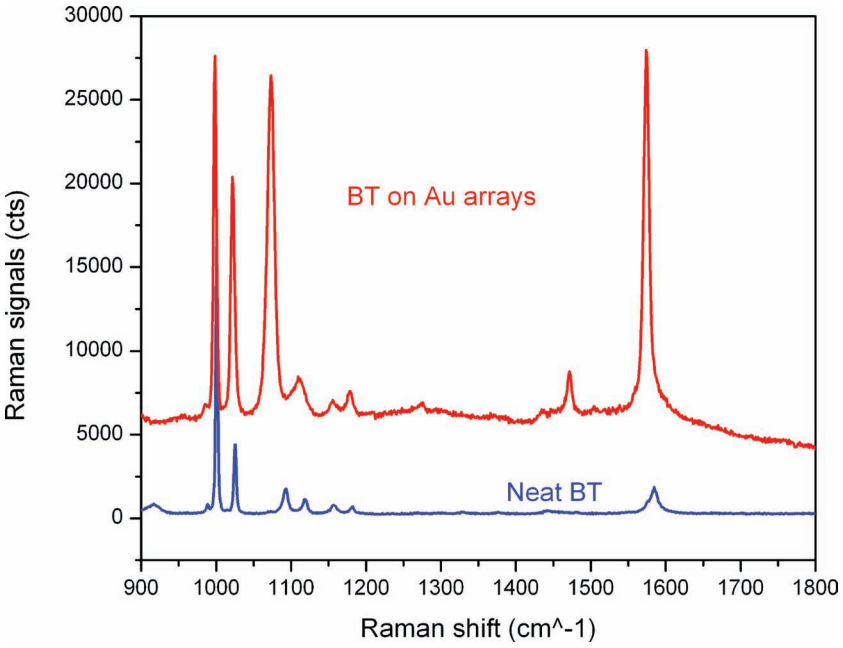

Figure 6. Raman signals from a monolayer of BT molecules deposited on 80 nm Au arrays (top line, 47 μW laser power, five acquisitions) and from neat BT (bottom line, 4.7 mW laser power, one acquisition).

enhancement factor was estimated from the comparison of this signal at the 1574 cm^{-1} line ($8a(a_1)$ C–C stretching mode of BT[31]) at 47 μW laser power and the same line at 4.7 mW laser power from neat BT in a cuvette (bottom curve in Figure 6). Traditional calculations of the number of molecules in appropriate excitation volumes and account of different excitation powers yields an average enhancement factor of $\approx 10^6$. The single-molecule enhancement in the hot spots analogous to that determined for the QDs above is $\approx 10^8$ if the hot spots are the main SERS source (see Experimental Section). In accordance with our FDTD calculations at 633 nm we considered that the large E^2 area is extended over an ≈5 nm spot around the minimum interparticle gap. Importantly, high-amplification hot spots are homogeneously distributed over the $1 \times 1.5\ \mu m^2$ excitation area, which provides the stability and fidelity of the Raman signal.

3. Conclusion

We have demonstrated a simple and cost-effective method to self-assemble 80 nm Au colloidal NPs into extended well-ordered structures. The large size of the NPs and the long-range order of arrays ensure high SERS and PL enhancement. Extinction spectra of our hcp Au NP crystals show strong interparticle coupling resulting in a distinct modification of their optical spectra and appearance of new resonance modes. These measurements are in a good agreement with the results of our FDTD simulations. The electromagnetic SERS enhancement factor of $\approx 10^4$ (at 514 nm excitation) and the PL enhancement of ≈10 are determined using 5 nm CdSe QDs as reporters on the Au NP arrays. By depositing BT molecular analytes in the interparticle gaps and using a larger excitation wavelength, we obtain much larger enhancement factors of $\approx 10^8$ associated with molecules in the hot spots. Ordered arrays of large noble-metal NPs could become the basis for new high-fidelity SERS sensors and nanophotonic devices requiring strong local light amplification and a high density of hot spots.

4. Experimental Section

Au NP Self-Assembly: Silicon wafers and microscope slides used as substrates were cleaned in oxygen plasma or in piranha solution (mixture of H_2SO_4/H_2O_2 = 3:1) at 120 °C for 10 min to remove organic contaminants and make the surface hydrophilic. Teflon ferrules (inner diameter ¼ inch) glued on the substrate with rubber cement were used to confine the NP solution. Au colloids (80 nm) were purchased from Ted Pella (original concentration $1.0 \times 10^{10}\ mL^{-1}$) and concentrated to $1.0 \times 10^{11}\ mL^{-1}$ in deionized water after 3× centrifugation at 1600 to 3000 rpm for 3 min in a 2-mL tube. Purified and concentrated Au NPs (50 μL) were injected into the Teflon ferrule and covered with a glass slip to reduce evaporation. Usually, it took from 2 to 3 days to evaporate all the liquid. We monitored the position of the NP array growth front with time and determined the speed of the monolayer and double-layer assembly as ≈0.1 and 0.03 μm s^{-1}, respectively (see SI).

Extinction Measurement and Raman Characterization: The UV–vis–near-infrared (NIR) extinction spectra at different points of the self-assembled Au arrays were measured using a modified microscope system and an Oriel MS257 spectrometer. A deuterium UV lamp and a wide-band halogen lamp were used for illumination. Raman spectra of CdSe QDs were measured using a Renishaw InVia Reflex Raman spectrometer with a 20× objective, 514 nm excitation wavelength, 80 μW power, ≈5 μm laser spot size, and 10 s integration time. Raman spectra of the BT molecules were collected in the same setup using a 50× objective at different powers of a 633 nm laser focused into a $1 \times 1.5\ \mu m^2$ spot (see SI, Figure S4). For consistent and repeatable results, all Raman measurements from Au arrays were acquired five times at 10 s integration.

Calculation of SERS Enhancement for Benzenethiol: The enhancement factor (EF) of a SERS substrate is determined as:[30]

$$EF = (I_{sub}/N_{sub})/(I_{vol}/N_{vol})$$

where I_{sub} and I_{vol} are Raman signals from BT on the substrate and neat BT, respectively. N_{sub} and N_{vol} are the numbers of molecules in appropriate excitation volumes. The excitation volume of the neat BT is defined by the size of the focused laser spot. The transverse dimensions of the laser spot were found experimentally by focusing it in the Raman setup on ≈450-nm-thick S1805 photoresist with different exposures. The wavelength of the 633 nm laser and 50× objective were the same as for the acquisition of the neat BT spectra. After exposure for 10 s at 100, 5, 1, and 0.1% of the full 4.7 mW laser power, the resist was developed and exposed spots were measured using SEM. Going from small underexposed (0.1%)

small NANO MICRO

to large overexposed (5 and 100%) pits allowed us to find the optimum spot size of ≈1.0 μm × 1.5 μm (Figure S4), which is close to the 0.8 μm theoretical focus size for our 50× objective (numerical aperture, NA = 0.75) at 633 nm wavelength. To determine the focus depth of our confocal microscope, we used an automated *Z* scan of the Raman system moving the cuvette with BT across the focal plane. The signal changed from zero when the focused beam was outside the cuvette to saturation when it was totally immersed in BT. From the $1/e^2$ profile of the scan we found the focal depth ≈10 μm. Therefore, the excitation volume = $(4\pi/3) \times 0.5 \times 0.75 \times 5\ (\mu m)^3 \approx 7.8 \times 10^{-12}\ cm^3$. Using the largest reported surface density of the BT monolayer on gold ($6.8 \times 10^{14}\ cm^{-2}$)[28–30] and the volume density of neat BT (1.0766 g cm^{-3}, or $5.855 \times 10^{21}\ cm^{-3}$ with molecular weight 110.73 g mol^{-1}), we obtained $N_{sub} \approx 1.6 \times 10^7$ and $N_{vol} \approx 4.6 \times 10^{10}$. After subtraction of the background and normalization to the same laser power, the ratio of Raman signals at the 1574 cm^{-1} line was ≈300. Thus, the average enhancement factor was $\approx 0.9 \times 10^6$. Our FDTD calculations showed that at 633 nm excitation the maximum electromagnetic field is confined in 5 nm spots around the smallest interparticle gaps and for the linear light polarization there is only one hot spot per particle. Accounting for the fact that the main Raman signal comes from BT molecules in the hot spots and estimating the number of molecules over these hot spots in the laser focus, the number of BT molecules located in the hot spot was only $\approx 6.3 \times 10^4$, which corresponded to a maximum of SERS $EF \approx 2.2 \times 10^8$.

Supporting Information

Supporting Information is available from the Wiley Online Library or from the author. It includes details of patterns formed during the capillary self-assembly of Au NPs under different conditions, the synthesis of CdSe QDs, the estimation of the photoluminescence, and the measurement of laser-focused spot size.

Acknowledgements

The submitted manuscript was created by UChicago Argonne, LLC, Operator of Argonne National Laboratory ("Argonne"). Argonne, a US Department of Energy Office of Science Laboratory, is operated under Contract No. DE-AC02-06CH11357.

[1] K. Kneipp, M. Moskovits, H. Kneipp, *Surface-Enhanced Raman Scattering*, Springer, Berlin/Heidelberg, **2006**.
[2] J. A. Dieringer, K. L. Wustholz, D. J. Masiello, J. P. Camden, S. L. Kleinman, G. C. Schatz, R. P. Van Duyne, *J. Am. Chem. Soc.* **2009**, *131*, 849–854.
[3] J. Beermann, S. M. Novikov, K. Leosson, S. I. Bozhevolnyi, *J. Opt. A: Pure Appl. Opt.* **2009**, *11*, 075004.
[4] J. P. Camden, J. A. Dieringer, J. Zhao, R. P. Van Duyne, *Acc. Chem. Res.* **2008**, *41*, 1653–1661.
[5] C. N. R. Rao, G. U. Kulkarni, P. J. Thomas, P. P. Edwards, *Chem. Soc. Rev.* **2000**, *29*, 27–35.
[6] Y. Wang, C. A. Mirkin, S.-J. Park, *ACS Nano* **2009**, *3*, 1049–1056.
[7] H. Ko, S. Singamaneni, V. V. Tsukruk, *Small* **2008**, *4*, 1576–1599.
[8] C. F. Bohren, D. R. Huffman, *Absorption and Scattering of Light by Small Particles*, Wiley-VCH, Weinheim, Germany **1998**.
[9] S. R. Emory, W. E. Haskins, S. Nie, *J. Am. Chem. Soc* **1998**, *120*, 8009–8010.
[10] Y. Wang, W. Zhou, *J. Nanosci. Nanotechnol.* **2010**, *10*, 1563–1583.
[11] H. Wang, C. S. Levin, N. J. Halas, *J. Am. Chem. Soc* **2005**, *127*, 14992–14993.
[12] N. D. Denkov, O. D. Velev, P. A. Kralchevsky, I. B. Ivanov, H. Yoshimura, K. Nagayama, *Nature* **1993**, *361*, 26.
[13] N. Denkov, O. Velev, P. Kralchevski, I. Ivanov, H. Yoshimura, K. Nagayama, *Langmuir* **1992**, *8*, 3183–3190.
[14] S. Watanabe, K. Inukai, S. Mizuta, M. T. Miyahara, *Langmuir* **2009**, *25*, 7287–7295.
[15] D. Bonn, J. Eggers, J. Indekeu, J. Meunier, E. Rolley, *Rev. Mod. Phys.* **2009**, *81*, 739–805.
[16] R. D. Deegan, *Phys. Rev. E* **2000**, *61*, 475–485.
[17] K. L. Kelly, E. Coronado, L. L. Zhao, G. C. Schatz, *J. Phys. Chem. B* **2003**, *107*, 668–677.
[18] K. L. Wustholz, A.-I. Henry, J. M. McMahon, R. G. Freeman, N. Valley, M. E. Piotti, M. J. Natan, G. C. Schatz, R. P. V. Duyne, *J. Am. Chem. Soc.* **2010**, *132*, 10903–10910.
[19] D. V. Talapin, A. L. Rogach, E. V. Shevchenko, A. Kornowski, M. Haase, H. Weller, *J. Am. Chem. Soc.* **2002**, *124*, 5782–5790.
[20] D. V. Talapin, J. H. Nelson, E. V. Shevchenko, S. Aloni, B. Sadtler, A. P. Alivisatos, *Nano Lett.* **2007**, *7*, 2951–2959.
[21] S. H. De Paoli Lacerda, J. F. Douglas, S. D. Hudson, M. Roy, J. M. Johnson, M. L. Becker, A. Karim, *ACS Nano* **2007**, *1*, 337–347.
[22] C. de Mello Donegá, S. G. Hickey, S. F. Wuister, D. Vanmaekelbergh, A. Meijerink, *J. Phys. Chem. B* **2003**, *107*, 489–496.
[23] O. Kulakovich, N. Strekal, A. Yaroshevich, S. Maskevich, S. Gaponenko, I. Nabiev, U. Woggon, M. Artemyev, *Nano Lett.* **2002**, *2*, 1449–1452.
[24] Y.-H. Chan, J. Chen, S. E. Wark, S. L. Skiles, D. H. Son, J. D. Batteas, *ACS Nano* **2009**, *3*, 1735–1744.
[25] M. C. Klein, F. Hache, D. Ricard, C. Flytzanis, *Phys. Rev. B* **1990**, *42*, 11123–11132.
[26] J. T. Hugall, J. J. Baumberg, S. Mahajan, *Appl. Phys. Lett.* **2009**, *95*, 141111.
[27] E. C. Le Ru, E. Blackie, M. Meyer, P. G. Etchegoin, *J. Phys. Chem. C* **2007**, *111*, 13794–13803.
[28] C. M. Whelan, M. R. Smyth, C. J. Barnes, *Langmuir* **1999**, *15*, 116–126.
[29] L.-J. Wan, M. Terashima, H. Noda, M. Osawa, *J. Phys. Chem. B* **2000**, *104*, 3563–3569.
[30] C. L. Haynes, R. P. Van Duyne, *J. Phys. Chem. B* **2003**, *107*, 7426–7433.
[31] T. H. Joo, M. S. Kim, K. Kim, *J. Raman Spectrosc.* **1987**, *18*, 57–60.

Received: April 10, 2011
Published online: June 1, 2011

